Carbohydrate Polymers 87 (2012) 2068–2075

Contents lists available at SciVerse ScienceDirect

Carbohydrate Polymers

journal homepage: www.elsevier.com/locate/carbpol

Biocompatible elastomer of waterborne polyurethane based on castor oil and polyethylene glycol with cellulose nanocrystals

Zhenzhong Gao [a], Jun Peng [b,*], Tuhua Zhong [c], Jin Sun [a], Xiaobo Wang [a], Chao Yue [a,**]

[a] Wood Science and Engineering Laboratory, South China Agriculture University, Guangzhou 510642, PR China
[b] Research Institute of Materials Science, South China University of Technology, Guangzhou 510640, PR China
[c] Division of Forestry and Natural Resources, West Virginia University, Morgantown, WV 26505, USA

ARTICLE INFO

Article history:
Received 3 September 2011
Received in revised form 3 October 2011
Accepted 12 October 2011
Available online 19 October 2011

Keywords:
Waterborne
Polyurethane
Cellulose
Nanocrystal
Reinforcement

ABSTRACT

Biocompatible waterborne polyurethane (WPU) based on castor oil (CO)/polyethylene glycol (PEG) filled with low level loadings of *Eucalyptus globulus* cellulose nanocrystals (ECNs) was prepared. The ECNs obtained by sulfuric hydrolysis, consisted of 'rod-like' crystals with an average length and diameter of 518.0 ± 183.4 nm and 21.7 ± 13.0 nm, respectively. The nanocomposites with low level loadings of ECNs showed significant enhancement in tensile strength and Young's modulus from 5.43 to 12.22 MPa and from 1.16 to 4.83 MPa, respectively. SEM results showed well dispersion of ECNs in the WPU matrix. Furthermore, it was verified that the nanosized ECNs favored the hard-segments (HSs)/soft-segments (SSs) microphase separation of the WPU, causing shifts of the SS glass transition temperature ($T_{g,s}$) and the HS melting temperature ($T_{m,h}$) toward higher temperatures.

1. Introduction

Biocompatible polymers, which derived from renewable resources such as vegetable oil (Tan & Chow, 2010), starch (Mathew, Thielemans, & Dufresne, 2008; Teixeira et al., 2011), soy protein (Wang, Cao, & Zhang, 2006), cellulose, with their non-toxic, biodegradable and eco-friendly advantages, are gaining extensive research attention. Moreover, there has been a growing trend in modifying bio-derived polymers with cellulose nanocrystals (CNs) to meet specific application ends or to get balanced properties. Composites with CNs as reinforcing fillers dispersing in polymer matrix, have shown significant enhancement in mechanical properties and thermal stability (Bras et al., 2010).

Cellulose nanocrystal, retrieved from lignocellulose through condensed acid hydrolysis, with its many remarkable properties such as high Young's modulus, high aspect ratio (Wu, Henriksson, Liu, & Berglund, 2007), low density, biocompatibility, biodegradability and so on, makes an ideal reinforcing filler in various polymer matrices, such as natural rubber (Azizi Samir, Alloin, & Dufresne, 2005; Bras et al., 2010), polypropylene (Ljungberg, Cavaillé, & Heux, 2006), poly (vinyl chloride), poly (lactic acid), polycaprolactone, silk fibroin, polyurethane, starch and soy protein plastics. In respect of CN, we generally refer to a particle derived from cellulose whose dimension is lower than 100 nm in at least one direction (Klemm et al., 2011; Siro & Plackett, 2010). As nano-filler, dimensions of these 'rod-like' crystals are related to the origins of cellulose and extraction conditions (Li & Ragauskas, 2011).

In the context of biocompatible polymer, waterborne polyurethane (WPU) is becoming one of the most popular polymers for availability of various application, health and environmental safety (Noble, 1997). Meanwhile, a large bulk of focus is placed on utilizing castor oil (CO) and polyethylene glycol (PEG) as raw materials in WPU synthesis due to their inherent biodegradability, low cost, socially favorable advantages and availability (Oprea, 2010). CO containing about 90% ricinoleic acid, is directly used as a tri-hydroxyl functioned monomer (Maafi, Tighzert, & Malek, 2010). In the mean time, PEG, known for good biocompatibility (Yoon, Kim, & Kim, 2005), has been extensively employed as low molecular weight diol for biodegradable PU synthesis. Therefore, WPU based on CO and PEG is considered as novel potential biomedical material for implants and tissue engineering (Cherian et al., 2011; Jiang et al., 2007; Liu, Zhong, Chang, Li, & Wu, 2010; Yeganeh & Hojatitalemi, 2007).

Aiming at the various applications, researchers endeavored to modify WPU with cellulose nanocrystal and other nanosized particles (Ayres, Orefice, & Sousa, 2006; Huang, Zou, Chang, Yu, & Dufresne, 2011; Kwon & Kim, 2005; Seo & Kim, 2005; Zhang, Wang, Zhao, Kang, & Wang, 2006; Zhang et al., 2008; Zou et al., 2011).

* Corresponding author. Tel.: +86 20 85294421; fax: +86 20 85294421.
** Corresponding author. Tel.: +86 20 85280264; fax: +86 20 85280264.
E-mail addresses: p.jun@mail.scut.edu.cn (J. Peng), ychao100@yahoo.com (C. Yue).

0144-8617/$ – see front matter © 2011 Elsevier Ltd. All rights reserved.
doi:10.1016/j.carbpol.2011.10.027

However, enhancement in mechanical properties like tensile strength and modulus is often accompanied by large reduction in extensibility and aggregations of the nanosized particles due to high loading levels (Auad, Mosiewicki, Richardson, Aranguren, & Marcovich, 2010; Cao, Dong, & Li, 2007; Goetz, Mathew, Oksman, Gatenholm, & Ragauskas, 2009; Ozgurseydibeyoglu & Oksman, 2008). To our knowledge, however, there still exists two critical challenges in nanocomposite reinforcement (Pei, Malho, Ruokolainen, Zhou, & Berglund, 2011). One is to obtain well dispersed reinforcing nanocrystals in polymer matrix, while the other is to increase the strength without notable decrease in their high extensibility.

In our present work, *Eucalyptus globulus* was introduced as the original resource of cellulose nanocrystal. *E. globulus* is a typical industrially farmed tree species, and it can sustainably provide cellulose nanocrystal raw material and has a great reinforcing potential (Besbes, Vilar, & Boufi, 2011; Syverud, Chinga-Carrasco, Toledo, & Toledo, 2011). Herein, with few relevant studies reported in literature (Chen et al., 2008; Pei et al., 2011), we introduced very low level loadings of *E. globulus* cellulose nanocrystals (ECNs) into the CO/PEG waterborne polyurethane (WPU) elastomer. Well dispersion of ECNs in the WPU matrix and significant reinforcement effect were obtained together with little reduction of elongation at break. The properties of the ultimate nanocomposite materials were systematically investigated by attenuated total reflection-Fourier transform infrared spectroscopy (ATR-FTIR), atomic force microscopy (AFM), differential scanning calorimetry (DSC), thermo gravimetric analysis (TGA) and tensile test. Morphology of the mixture films was characterized by scanning electron microscopy (SEM).

2. Experimental

2.1. Raw materials

E. globulus chips were kindly supported by Guangdong DongJiang forest farm. Isophorone diisocyanate (IPDI) was obtained from Bayer AG. Castor oil (CO) (hydroxyl value = 163 mg KOH/g) was obtained from Guangdong Guanghua Chemical Factory Co., Ltd. Polyethylene glycol (PEG) (M_n = 2000) was obtained from Shanghai Qiangshun Chemical Factory Co., Ltd. CO and PEG were stored and dried under vacuum for 72 h. Dimethylol propionic acid (DMPA) was obtained from Perstorp Co., Sweden. Dibutyltin dilaurate (DBTDL) was obtained from Shanghai Lingfeng Chemical Reagent Co., Ltd. 1, 4-Butanediol (BD), N-methyl-2-pyrrolidone (NMP), triethylamine (TEA) and ethylenediamine (EDA) were obtained from Kermel Chemical Co., Ltd.

2.2. Preparation of ECNs

Eucalyptus chips with random sizes smaller than 5 cm were dumped into a grinder to obtain dry powders. The particles that passed through a 40-mesh sieve (355 μm), but retained by a 60-mesh sieve (250 μm), were obtained as *E. globulus* samples and packed in plastic bag at ambient temperature. Cellulose fiber was extracted from the *E. globulus* samples using the HNO_3–$KClO_3$ method (Liu et al., 2010b). The powder was immersed in 30% nitric acid aqueous solution. $KClO_3$ was added into the solution at a 10 wt.% ratio based on the weight of nitric acid. The weight ratio of *E. globulus* powder was about 10 wt.%. After extracting for 24 h at 80 °C, the obtained fiber suspension was cooled and placed in regenerated cellulose dialysis membranes (MWCO of 14,000) and dialyzed against distilled water for 72 h to remove low molecular weight compounds. The slurry was then freeze-dried. The yield of dry cellulose fiber in relation to the original *E. globulus* powder is approximately 35%. CNs were produced via further hydrolysis. Sulfuric acid (65%) was mixed with the cellulose fiber under continuous stirring at a temperature of 40 °C for 2 h and then the sulfuric acid and the hydrolysate were washed off by dialysis in distilled water. After further dilution, a 0.5% suspension was prepared and stored for film preparation and analysis.

2.3. Synthesis of WPU

The synthesis of CO/PEG waterborne polyurethane is through a prepolymer mixing process (Dieterich, 1981). The NCO/OH value of the prepolymer is 1.4. The weight percentage of DMPA is 6% in relation to the entire solid weight. The process of the polyaddition reaction is depicted as follows. CO (15.75 g) and PEG (11.44 g) were put into a round bottom, four necked flask equipped with a nitrogen inlet, a condenser with a drying tube, a mechanical Teflon stirrer and a thermometer. The round bottom flask was put in an oil bath to get even heat distribution. Under continuous stirring, the mixture was heated to 120 °C to dehydrate under vacuum for 3 h. Then the temperature is lowered to 60 °C, IPDI (22.23 g) was added into the flask. DBTDL (0.3 wt.% with respect to IPDI) was injected into the reactant, and then the reaction lasted for 1 h. After that, the reaction temperature was raised to 70 °C, when the DMPA (3.34 g) and BD (1.19 g) dissolved in NMP were charged into the flask to react for 2 h. The NCO% value of the prepolymer was determined using a standard of ASTM D2572-97, when the NCO content reached a theoretical value, the reaction temperature was lowered to 50 °C, TEA (2.26 g) was then added into the prepolymer to neutralize the carboxyl group for 0.5 h. Then the anionomer was emulsified by a high speed emulsifying machine with distilled water slowly charged in. EDA (1.71 g) diluted in distilled water was added to extend the polymer chain during the emulsification. Finally, the CO/PEG WPU emulsion with about 50 wt.% HS content (with respect of total WPU solid weight) was obtained.

2.4. Preparation of WPU/ECNs nanocomposite films

ECNs dilute dispersion was ultrasonicated for 10 min to avoid agglomeration. Then, the suspension of nanocrystals and WPU was mixed with the absolute ECNs contents of 0.2, 0.5, 1, 2, 3, 4, 5 wt.% in relation to WPU. The blend was magnetically stirred for 3 h. After that, the obtained mixture was degassed under vacuum at ambient temperature. Subsequently, the mixture was cast into a polystyrene square Petri dish and vacuum-dried at 45 °C for 1 week. The nanocomposite films with a mean thickness of 0.25 mm were obtained and stored in a desiccator with 0% relative humidity.

2.5. Characterization

An atomic force microscopy (AFM) instrument (Veeco SPM IIIA, US) with an AFFM scanner working in multi-mode was used to collect stereoscopic information of the ECNs. A droplet of diluted ECNs suspension was coated on a flake of mica, and dried under vacuum over night. The AFM image was exported in Height-Mode.

Morphology observation of the nanocomposite films was carried out on a field emission scanning electron microscope, FE-SEM (Sirion 200, FEI, The Netherlands). The specimens were frozen in liquid nitrogen, fractured, and coated with gold by an ion sputter coater and were observed under FE-SEM operating at 12.5 kV.

ATR-FTIR spectroscopy was performed on a PerkinElmer Spectrum 100 spectrometer at ambient temperature. An ATR sampling accessory (THE PIKE MIRACLETM) with a ZnSe crystal was outfitted. The samples from the film were cut off randomly and placed flat on the crystal surface. The spectra were automatically recorded over 128 scans with a resolution of 2 cm^{-1}. The background spectrum was previously recorded with contacting air on the crystal surface.

Differential scanning calorimetry (DSC) measurement of the nanocomposite films was performed on a DSC 204C instrument (Netzsch Co., Germany) under nitrogen atmosphere. Scans were carried out at a heating rate of 10 K min^{-1} within a range from −80 to 250 °C. The glass transition temperature was recorded as the midpoint of the heat capacity change.

Thermal stability of the films was tested on a TGA 209F3 (Netzsch Co., Germany) apparatus to get information about weight loss during heating. Samples of about 10 mg were separately heated from 30 to 550 °C under nitrogen atmosphere, with a heating rate of 10 K min^{-1}.

The mechanical properties including tensile strength (σ_b), elongation at break (ε_b), and Young's modulus (E) of the nanocomposite films with dimensions of 50 mm × 10 mm × 0.25 mm (length × width × thickness) were carried out on a universal testing machine (SUNS CMT5504, Shenzhen) with a loading rate of 100 mm min^{-1} according to the standard of ISO 527-3:1996 (E) at room temperature. An average value of five replicates of each sample group was taken.

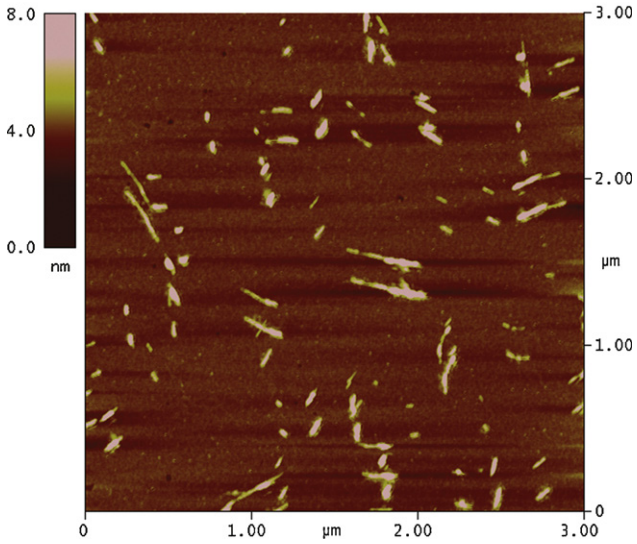

Fig. 1. AFM image of dilute ECNs suspension.

3. Results and discussion

3.1. Morphology of ECNs nanocomposite films

The AFM image of the ECNs in dilute suspension is shown in Fig. 1, from which both individual and slightly aggregated cellulose nanocrystals were observed. Using the built-in measurement tool of the imaging software, we have got the geometric data of the ECNs. These 'rod-like' crystals have a wide distribution in dimension, from 304.7 to 880.63 nm in length and from 6.6 to 45.0 nm in diameter. The average length and diameter were 518.0 ± 183.4 nm and 21.7 ± 13.0 nm, respectively. Therefore, the aspect ratio (L/D) of the ECNs was 23.87 approximately. Cellulose nanocrystals with a high aspect ratio like this contribute to the low percolation threshold. This predicts a low loading level of ECNs filler in the WPU polymer matrix.

Fig. 2A–D showed the SEM images of the frozen-fractured surfaces of the WPU/ECNs nanocomposite films. It can be informed that with ECNs content increasing from 0 to 5 wt.%, the advancing cracks of the pure WPU film (Fig. 2A), are increasingly deflected

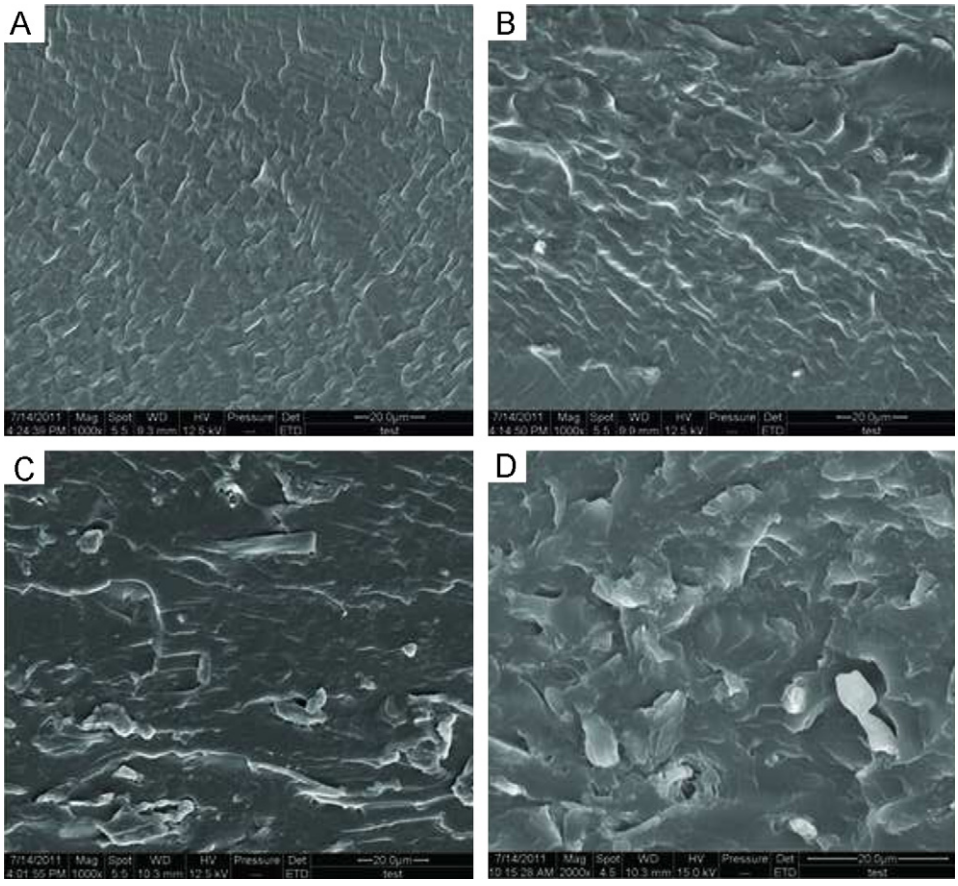

Fig. 2. SEM images of the ECNs/WPU nanocomposite films with different ECNs content: (A) 0 wt.%; (B) 1 wt.%; (C) 3 wt.%; (D) 5 wt.% (scale bar: 20 μm).

Table 1
Curve-fitting results of ECNs/WPU nanocomposites FTIR spectra in N–H region.

Samples	Peak I[a]			Peak II		
	Location	Area	$W_{1/2}$[b]	Location	Area	$W_{1/2}$
WPU	3334.6	4.62	166.0	3525.7	0.82	123.1
WPU-0.2	3334.3	5.12	169.8	3524.7	0.94	126.1
WPU-0.5	3336.4	5.10	169.0	3525.6	1.02	128.0
WPU-1.0	3336.1	4.91	166.5	3527.0	0.90	129.1
WPU-2.0	3338.1	5.62	170.5	3525.9	1.22	133.3
WPU-3.0	3337.0	5.53	169.5	3527.5	1.14	134.8
WPU-4.0	3336.0	6.39	173.9	3527.7	1.17	137.2
WPU-5.0	3335.4	6.23	174.2	3527.4	1.29	141.1

[a] Peak I, hydrogen bonded N–H stretching; Peak II, free N–H stretching (there exists embedded peaks in Peak II, see also in Section 3.2.1).
[b] $W_{1/2}$, band width at height of the peak.

and tortured (Fig. 2C–D), indicating a more complicated energy dissipating mechanism within the interfaces between ECNs and the WPU matrices. The cellulose nanocrystals were identified as small white dots in the fractured surfaces of the film. The white dots could correspond to the nanocrystals in the perpendicular plane of the films (Cao et al., 2007). Roughening showed uniform distribution all over the fractured surface, indicating well distribution of ECNs in the WPU. As we know, well dispersion of ECNs combined with strong interactions between fillers and the matrix are among the essential requirement for improving the mechanical properties and thermal stability of WPU.

3.2. Characterization of hydrogen bonding via ATR-FTIR

The specific structural feature of WPU elastomer is their two-phase microstructure which is the result of thermodynamic incompatibility between hard urethane or urea segments and soft polyester or polyether segments. The extent of the micro-phase separation is essential to a WPU elastomer of good mechanical properties (Bistričić, Baranović, Leskovac, & Bajsić, 2010). Hydrogen bonds are important physical interactions affecting the micro-phase separation in WPU, determining the microstructure, as well as the mechanical and thermal properties of the polymer (Li et al., 2009; Yoon, Sung, & Ratner, 1990). Multiple hydrogen bonds can be formed between polar groups where one group serves as a proton 'donor', while the other servers as a proton 'acceptor'. For the WPU in our study, there existed two different kinds of proton 'donors' (urethane N–H and urea N–H) and four kinds of proton 'acceptors' (urethane C=O, urea C=O, ester C=O of castor oil and C–O–C of PEG) (Luo, Wang, & Ying, 1997; Senich & MacKnight, 1980). Moreover, the O-H introduced by ECNs can have strong interactions with the WPU matrix (Cao et al., 2007). There are several vibrational modes that are sensitive to hydrogen bonding in polyurethane, however, the most information can be obtained from the N–H and C=O stretching modes at 3600–3100 and 1600–1760 cm^{-1}, respectively. Fig. 3 shows the whole FTIR spectra of the ECNs/WPU nanocomposites with pure WPU as reference. To gain insight into the fact that how ECNs affected hydrogen bonding in the WPU matrix, detailed curve-fitting procedures were carried out related to spectra in N–H and C=O regions, respectively.

3.2.1. N–H stretching region

The N–H stretching region of each spectrum shows the hydrogen bonded (Peak I) and free (Peak II) bands near 3335 and 3527 cm^{-1}, respectively. The peak envelope was fitted into two Gaussian bands (Mattia & Painter, 2007) as Fig. 4A, in spite that the absorption of O–H in cellulose nanocrystals are embedded in the shoulder peak. The curve-fitting results are listed in Table 1. Two main parameters of the nanocomposites, band area and width at half height of the peak, were measured. With increase of cellulose

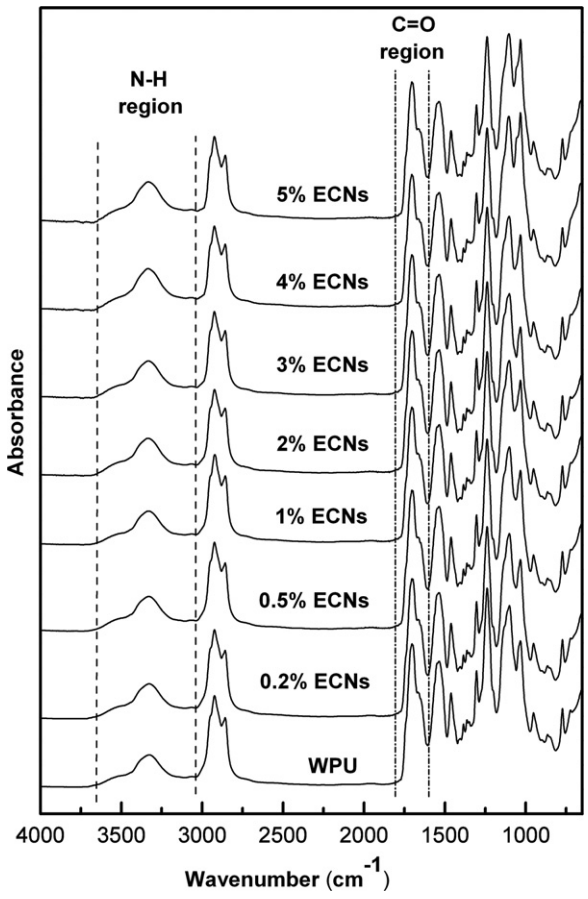

Fig. 3. ATR-FTIR spectra of the ECNs/WPU nanocomposite films with the pure WPU as reference.

content, the band area of Peak I increased, but not monotonically. This can be attributed to two opposite contributions. For one thing, dissociation of the original hydrogen bond associated with the N–H of WPU matrix caused a decreasing trend. For another, introducing of ECNs into the WPU matrix led to newly formed hydrogen bonds between C=O and O–H on the surface of cellulose nanocrystals, which contributed to the increasing trend of band area. Therefore, the overall area increase indicates that more hydrogen bonds formed due to adding ECNs into the WPU matrix, while there is less cleavage of the original hydrogen bonds in the WPU matrix. For Peak II, there was also to some extent an increase. This might be explained that the ECNs enhanced the microphase separation between HSs and SSs, giving the soft chains more freedom whose C=O and C–O–C could have initially hydrogen bonded to the N–H of the HSs. At the same time, the broadening of the band shapes indicates a wider distribution of hydrogen bond due to additional proton 'donor' of the ECNs' O–H group.

3.2.2. C=O stretching region

The C=O stretching region can be quantitively identified to characterize hydrogen bonding (Coleman, Skrovanek, Hu, & Painter, 1988; Yoon et al., 1990). Herein, there are three factors making the C=O region very complex. Firstly, there are two kinds of C=O (*urethane* C=O and *urea* C=O) in the HSs. Secondly, the ester C=O of castor oil also have a band location within this region (Maafi et al., 2010), overlapped with that of urethane C=O. Lastly, the C=O of DMPA also showed its absorption peak around 1660 cm^{-1} overlapping the *urea disordered* hydrogen bonded C=O peak (Kwak, Kim, Ha Yoo, & Kim, 2004). Nonetheless, the whole band envelope can

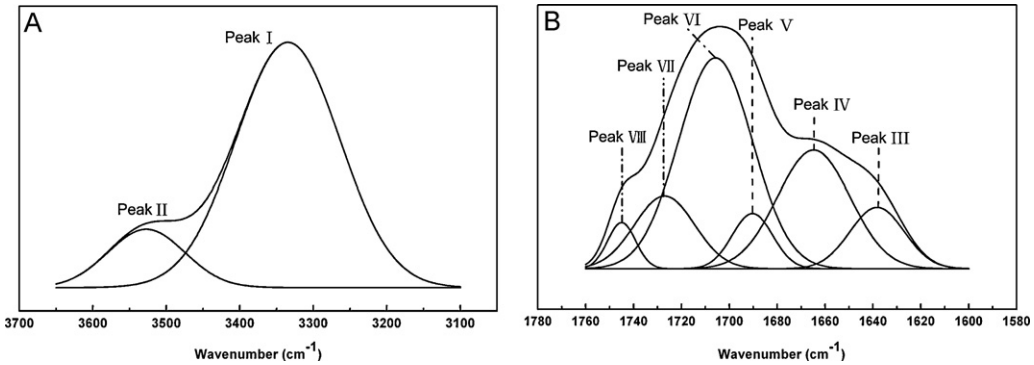

Fig. 4. Curve-fitting of FTIR spectrum in N–H region (A) and C=O region (B).

Table 2
Curve-fitting results of ECNs/WPU nanocomposites FTIR spectra in C=O region.

Samples	C=O stretching region of urea group						C=O stretching region of urethane group					
	[a] Peak III		Peak IV		Peak V		Peak VI		Peak VII		Peak VIII	
	Location (cm^{-1})	Area	Location (cm^{-1})	Area	Location (cm^{-1})	Area	Location (cm^{-1})	Area	Location (cm^{-1})	Area	Location (cm^{-1})	Area
WPU	1638.3	0.86	1664.8	2.22	1690.3	0.57	1705.8	4.02	1726.9	1.13	1744.9	0.33
WPU-0.2	1638.3	0.81	1664.7	2.60	1690.4	0.46	1705.7	3.87	1727.0	1.05	1744.8	0.35
WPU-0.5	1638.2	0.82	1664.8	2.29	1690.3	0.51	1705.8	3.75	1726.9	1.16	1744.9	0.33
WPU-1.0	1638.2	0.71	1664.8	2.28	1690.4	0.48	1705.8	3.77	1726.9	1.08	1744.8	0.35
WPU-2.0	1638.3	0.89	1664.7	2.34	1690.3	0.52	1705.8	3.88	1726.9	1.24	1744.9	0.33
WPU-3.0	1638.3	0.76	1664.8	2.49	1690.4	0.51	1705.7	3.61	1727.0	1.33	1744.8	0.34
WPU-4.0	1638.2	0.60	1664.8	2.45	1690.3	0.45	1705.8	3.39	1726.9	1.22	1744.9	0.35
WPU-5.0	1638.3	0.59	1664.7	2.58	1690.3	0.42	1705.8	3.36	1726.9	1.33	1744.9	0.34

[a] Peak III and Peak IV, Hydrogen bonded C=O stretching of *urea group*, ordered and disordered, respectively; Peak V, free C=O stretching of *urea group*; Peak VI and Peak VII, Hydrogen bonded C=O stretching of *urethane group*, ordered and disordered, respectively. Peak VIII, free C=O stretching of *urethane group* (there exists embedded peaks in Peak IV, VII Peak and Peak VIII, see also in Section 3.2.2).

be decomposed into six Gaussian bands through a curve-fitting procedure. Fig. 4B shows the curve-fitted spectrum in the region at 1760–1600 cm^{-1}. The peaks centered at around 1638 cm^{-1} and 1705 cm^{-1} are assigned to the *urea* and *urethane ordered* hydrogen bonded C=O, respectively. The peak centered around 1690 and 1744 cm^{-1} are assigned to the *free urea* and *urethane* C=O of hard segments, respectively. The peak centered at around 1664 cm^{-1} arouse from *urea disordered* hydrogen bonded C=O, with embedded DMPA C=O peak. The peak at around 1726 cm^{-1} is assigned to *urethane disordered* hydrogen bonded C=O. Additionally, the C=O of castor oil of the soft-segment may have similar absorption peaks embedded in *urethane free* and *disordered* hydrogen bonded C=O absorption peaks. The curve-fitting results are summarized in Table 2. The *urea* hydrogen bond is sensitive to the changes within the hard domain, while the urethane hydrogen bond is sensitive to the changes on the HSs/SSs interface (Bummer & Knutson, 1990). As presented in the table, adding cellulose nanocrystals decreased the band area in *urea ordered* hydrogen bonding C=O (Peak III) and the band area in *urethane ordered* hydrogen bonding C=O (Peak VI), while slightly increased band areas of both *disordered* hydrogen bonded absorption peaks (Peak IV and Peak VII), indicating that the ECNs largely formed new hydrogen bond with the HSs of the WPU matrix. This fact may account for that only a little decrease in elongation at break occurred when low loading of cellulose nanocrystals reinforced the WPU matrix. Moreover, in spite of perturbation and overlapping effect, we could also see a descending of area data in *urea free* C=O (Peak V), and we believed in that there also existed a similar trend in *urethane free* C=O (Peak VIII), while masked by the increasing of free ester C=O of castor oil in SSs. Herein, the increasing of free ester C=O of castor oil of SSs is the result of enhanced microphase separation mentioned in Section 3.2.1.

3.3. Mechanical properties

Nanocomposite films with different contents of ECNs were tested under uniaxial extension at room temperature and the results for the their mechanical properties including tensile strength (σ_b), elongation at break (ε_b), and Young's modulus (E) are presented in Fig. 5 and Table 3, with the pure WPU as reference. The pure WPU film possessed typical rubbery modulus and high elongation at break of an elastomer: a low tensile strength of 5.43 MPa and a low Young's modulus of 1.16 MPa as well as a high elongation of 381.72%. From Table 3, we can see that the reinforcement effect on the tensile properties is remarkable relative to the nanofiller contents. The tensile strength (σ_b) and Young's modulus (E) of the films increased simultaneously at loadings below 1 wt.%. The σ_b increased significantly from 5.43 to 12.22 MPa with the increasing filler content from 0 to 1 wt.% and then decreased continuously (still higher than that of pure WPU) at loadings above 1 wt.%. It is worth noting that σ_b of the 1 wt.% sample is the highest, suggesting a well homodispersion of the hydrophilic ECNs in the WPU matrix. With

Table 3
Mechanical properties of CO/PEG WPU and its nanocomposite films.

Samples	Tensile strength (σ_b) (MPa)	Elongation at break (ε_b) (%)	Young's modulus (E) (MPa)
WPU	5.42 ± 0.26	381.72 ± 22.33	1.16 ± 0.10
WPU-0.2	6.03 ± 0.33	355.92 ± 18.37	2.44 ± 0.14
WPU-0.5	8.10 ± 0.45	386.35 ± 9.40	2.37 ± 0.16
WPU-1.0	12.22 ± 0.52	370.68 ± 16.85	2.30 ± 0.12
WPU-2.0	9.62 ± 0.82	361.55 ± 15.13	2.76 ± 0.13
WPU-3.0	7.99 ± 0.53	354.85 ± 10.40	3.14 ± 0.42
WPU-4.0	8.09 ± 0.33	303.26 ± 17.70	4.83 ± 0.14
WPU-5.0	6.56 ± 0.28	303.55 ± 16.63	3.44 ± 0.30

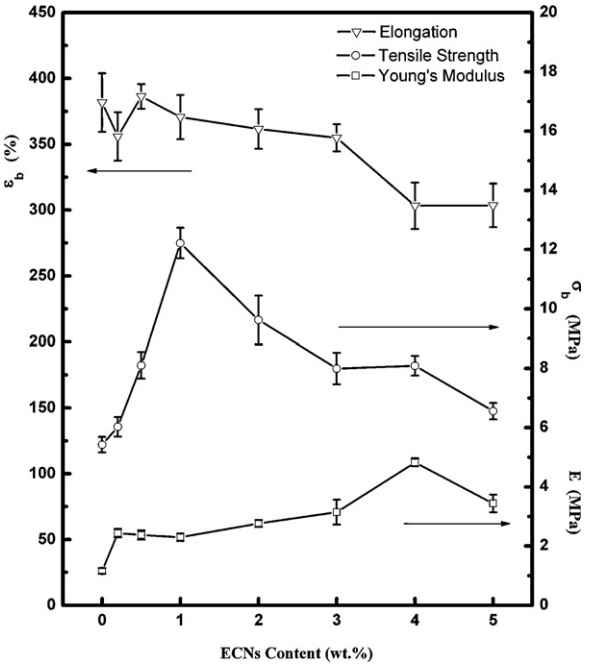

Fig. 5. Effect of ECNs content on tensile strength (σ_b), Young's modulus (E) and elongation at break (ε_b) of the nanocomposite films compared with the pure WPU (the σ_b and the E share the same right axis).

upraised ECNs contents, there might be some self-aggregations that reduce the interface area between the ECNs and the polymer matrix relative to the overall surface area of ECNs, resulting in lowering of hydrogen bonding density and transferring stress deficiency. At the same time, the E increased from 1.16 to 4.83 MPa with a increasing filler content from 0 to 4 wt.%, followed by a decrease, which can be explained by the above-mentioned percolation threshold model, showing excess loading of nanofiller would exert adverse impact on the modulus of the polymer. In our work, the volume fraction of the ECNs reached to a percolation threshold (V_{TH}), which depends on the aspect ratio of the ECNs and can be calculated by $V_{TH} = 0.7/(L/D)$ (Cao et al., 2007; Favier, Chanzy, & Cavaille, 1995). Herein, we substituted 23.87 for the value of L/D into the above equation, and the results were V_{TH} = 2.93 vol.%, 4.07 wt.%, taking 1.5 and 1.08 g cm^{-3} for the density of crystalline cellulose and the WPU matrix, respectively (Cao & Zhang, 2005; Noble, 1997). Interestingly, the nanocomposite films displayed elongations at break (ε_b) higher than 300% with no significant reduction compared with the pure WPU. This is also attributed to the majority of new hydrogen bonding in the HSs/ECNs interface, enhancing microphase separation, which is consistent with the results of the FTIR tests.

3.4. Thermal analysis

DSC thermograms and corresponding data for all the nanocomposite samples including pure WPU are shown in Fig. 6 and listed in Table 4, respectively. The figure refers to the first heating step, which shows a few endothermic peaks at high temperatures, probably the results of incomplete phase separation and formation of domains with different degrees of order. However, it can be clearly seen that the glass-transition temperatures of the SS as well as the melting of the HS. Herein, there exists cold crystallization and crystal perfection during the whole heating procedure, for example, the exothermic peak around −10 °C. The data in Table 4 showed an increasing trend of the $T_{g,s}$ of the SS on the whole, as well as the melting temperature of the HS ($T_{m,h}$). This indicates that the adding of ECNs favored the microphase separation between HS and

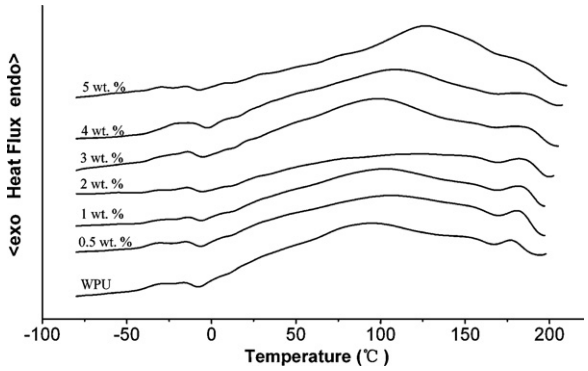

Fig. 6. DSC thermograms of pure WPU and different nanocomposites.

Table 4
Thermal properties of the ECNs/WPU nanocomposite films.

Sample	$T_{g,s}$ (°C)[a]	$T_{m,h}$ (°C)	$T_{30\%}$ (°C)[b]
WPU	−35.5	178.9	312.4
WPU-0.5	−36.6	181.3	317.2
WPU-1.0	−35.3	181.5	317.9
WPU-2.0	−34.4	181.9	318.6
WPU-3.0	−35.0	183.4	320.2
WPU-4.0	−34.6	188.1	320.0
WPU-5.0	−34.3	193.0	320.1

[a] DSC results: $T_{g,s}$, glass transition temperature of soft-segments; $T_{m,h}$, melting temperature of hard-segment.
[b] TGA results: $T_{30\%}$, temperature at 30% weight loss.

SS. The $T_{g,s}$ variation is very little with 0–1 wt.% ECNs, however, which means insufficient ECNs filler content to affect the $T_{g,s}$ of the SSs. As expected, the $T_{g,s}$ increased at loadings of ECNs above 1 wt.%, indicating perfection of more crystals or higher crystallinity over enhanced microphase separation, where the ECNs might serve as nucleating agents (Auad, Contos, Nutt, Aranguren, & Marcovich, 2008). This is also proved by the shift of $T_{m,h}$ towards higher temperature.

Fig. 7 shows the thermograms of TGA measurement for the pure WPU and different nanocomposite films. The thermal degradation temperatures of 30% weight loss ($T_{30\%}$) are summarized in Table 4. Two successive weight loss processes for all the samples were observed, corresponding to HS thermal degradation at lower temperature and SS degradation at higher temperature. The temperature of 30% weight loss shifted from 312.4 °C for the pure WPU to 320.1 °C for the WPU containing 5 wt.% ECNs. It is informed that the WPU polymer matrices containing ECNs possessed higher heat resistance during the hard-segment decomposition. Thermal

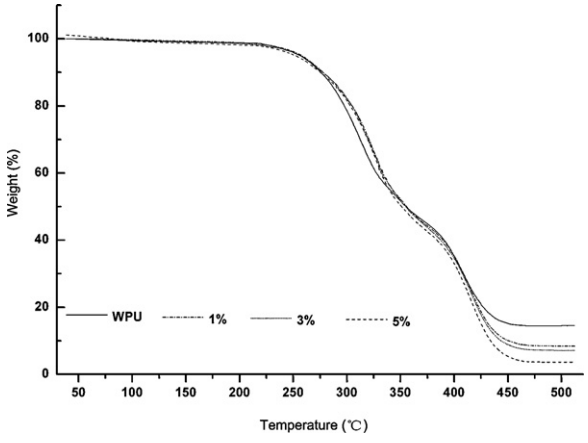

Fig. 7. TGA thermograms of pure WPU and different nanocomposites.

stability of the HSs was enhanced. This is attributed to the synergistic effect of thermal stability of ECNs and hydrogen bond with the HSs, which is in good agreement with the results of the FTIR measurement. While at higher temperatures during the soft-segment decomposition, it is hard to tell enhancements among all the samples. The decrease of final thermal degradation residue weight can be easily explained that cellulose nanocrystals have no more than 2 wt.% residue at higher temperature(Köll, Borchers, & Metzger, 1991). Therefore, increase of ECNs content reduced the WPU weight, leading to low residue weight of the samples.

4. Conclusion

Uniform distribution of ECNs in the WPU matrix and significant reinforcement were achieved due to low loadings of ECNs and strong hydrogen bonding between polymer matrix and filler. Nanoscale structural changes characterized by ATR-FTIR test shows that incorporation of ECNs favors the microphase separation between HSs and SSs, while new ECNs/WPU hydrogen bonding formed largely within the hard domain, leading to higher hydrogen bond density in hard domain and less reduction of elongation at break. A low level loading of 1 wt.% ECNs significantly enhanced the tensile strength from 5.43 to 12.22 MPa, while the Young's modulus reached the maximum of 4.83 MPa at a loading of 4 wt.% ECNs. At the same time, thermal stability of the WPU was enhanced within the HS degradation temperature range.

The results have shown that CN from *E. globulus* exhibits excellent reinforcement effect on WPU polymer due to its rigid nature and high aspect ratio, as well as hydrophily.

Acknowledgements

Laboratory of Wood Science and Engineering, South China Agriculture University (SCAU) has been greatly acknowledged for financial support and supplied raw materials. The author would also like to thank Cui Yongzhi, Materials Science and Engineering College, Northeast Forestry University for technical support.

References

Auad, M. L., Contos, V. S., Nutt, S., Aranguren, M. I. & Marcovich, N. E. (2008). Characterization of nanocellulose-reinforced shape memory polyurethanes. *Polymer International*, *57*, 651–659.

Auad, M. L., Mosiewicki, M. A., Richardson, T., Aranguren, M. I. & Marcovich, N. E. (2010). Nanocomposites made from cellulose nanocrystals and tailored segmented polyurethanes. *Journal of Applied Polymer Science*, *115*, 1215–1225.

Ayres, E., Orefice, R. L. & Sousa, D. (2006). Influence of bentonite type in waterborne polyurethane nanocomposite mechanical properties. *Macromolecular Symposia*, *245*, 330–336.

Azizi Samir, M. A. S., Alloin, F. & Dufresne, A. (2005). Review of recent research into cellulosic whiskers, their properties and their application in nanocomposite field. *Biomacromolecules*, *6*, 612–626.

Besbes, I., Vilar, M. R. & Boufi, S. (2011). Nanofibrillated cellulose from Alfa, Eucalyptus and Pine fibres: Preparation, characteristics and reinforcing potential. *Carbohydrate Polymers*, *86*, 1198–1206.

Bistričić, L., Baranović, G., Leskovac, M. & Bajsić, E. G. (2010). Hydrogen bonding and mechanical properties of thin films of polyether-based polyurethane–silica nanocomposites. *European Polymer Journal*, *46*, 1975–1987.

Bras, J., Hassan, M. L., Bruzesse, C., Hassan, E. A., El-Wakil, N. A. & Dufresne, A. (2010). Mechanical, barrier, and biodegradability properties of bagasse cellulose whiskers reinforced natural rubber nanocomposites. *Industrial Crops and Products*, *32*, 627–633.

Bummer, P. M. & Knutson, K. (1990). Infrared spectroscopic examination of the surfaces of hydrated copoly(ether-urethane-ureas). *Macromolecules*, *23*, 4357–4362.

Cao, X. & Zhang, L. (2005). Effects of molecular weight on the miscibility and properties of polyurethane/benzyl starch semi-interpenetrating polymer networks. *Biomacromolecules*, *6*, 671–677.

Cao, X. D., Dong, H. & Li, C. M. (2007). New nanocomposite materials reinforced with flax cellulose nanocrystals in waterborne polyurethane. *Biomacromolecules*, *8*, 899–904.

Chen, G., Wei, M., Chen, J., Huang, J., Dufresne, A. & Chang, P. R. (2008). Simultaneous reinforcing and toughening: New nanocomposites of waterborne polyurethane filled with low loading level of starch nanocrystals. *Polymer*, *49*, 1860–1870.

Cherian, B. M., Leão, A. L., de Souza, S. F., Costa, L. M. M., de Olyveira, G. M., Kottaisamy, M., et al. (2011). Cellulose nanocomposites with nanofibres isolated from pineapple leaf fibers for medical applications. *Carbohydrate Polymers*, *86*, 1790–1798.

Coleman, M. M., Skrovanek, D. J., Hu, J. & Painter, P. C. (1988). Hydrogen bonding in polymer blends. 1. FTIR studies of urethane-ether blends. *Macromolecules*, *21*, 59–65.

Dieterich, D. (1981). Aqueous emulsions, dispersions and solutions of polyurethanes; synthesis and properties. *Progress in Organic Coatings*, *9*, 281–340.

Favier, V., Chanzy, H. & Cavaille, J. Y. (1995). Polymer nanocomposites reinforced by cellulose whiskers. *Macromolecules*, *28*, 6365–6367.

Goetz, L., Mathew, A., Oksman, K., Gatenholm, P. & Ragauskas, A. (2009). A novel nanocomposite film prepared from crosslinked cellulosic whiskers. *Carbohydrate Polymers*, *75*, 85–89.

Huang, J., Zou, J. W., Chang, P. R., Yu, J. H. & Dufresne, A. (2011). New waterborne polyurethane-based nanocomposites reinforced with low loading levels of chitin whisker. *Express Polymer Letters*, *5*, 362–373.

Jiang, X., Li, J., Ding, M., Tan, H., Ling, Q., Zhong, Y., et al. (2007). Synthesis and degradation of nontoxic biodegradable waterborne polyurethanes elastomer with poly(-caprolactone) and poly(ethylene glycol) as soft segment. *European Polymer Journal*, *43*, 1838–1846.

Klemm, D., Kramer, F., Moritz, S., Lindstrom, T., Ankerfors, M., Gray, D., et al. (2011). Nanocelluloses: A new family of nature-based materials. *Angewandte Chemie International Edition*, *50*, 5438–5466.

Köll, P., Borchers, G. & Metzger, J. O. (1991). Thermal degradation of chitin and cellulose. *Journal of Analytical and Applied Pyrolysis*, *19*, 119–129.

Kwak, Y. S., Kim, E. Y., Ha Yoo, B. & Kim, H. D. (2004). Preparation and properties of waterborne poly(urethane urea)s for adhesives: The effects of the 2,2-bis(hydroxylmethyl)propionic acid content on the properties. *Journal of Applied Polymer Science*, *94*, 1743–1751.

Kwon, J. & Kim, H. (2005). Comparison of the properties of waterborne polyurethane/multiwalled carbon nanotube and acid-treated multiwalled carbon nanotube composites prepared by in situ polymerization. *Journal of Polymer Science Part A: Polymer Chemistry*, *43*, 3973–3985.

Li, Q., Zhou, H., Wicks, D. A., Hoyle, C. E., Magers, D. H. & McAlexander, H. R. (2009). Comparison of small molecule and polymeric urethanes, thiourethanes, and dithiourethanes: Hydrogen bonding and thermal, physical, and mechanical properties. *Macromolecules*, *42*, 1824–1833.

Li, Y. & Ragauskas, A. J. (2011). Cellulose nano whiskers as a reinforcing filler in polyurethanes. In Boreddy Reddy (Ed.), *Advances in diverse industrial applications of nanocomposites* , ISBN 978-953-307-202-9. InTech. Available from: http://www.intechopen.com/articles/show/title/cellulose-nano-whiskers-as-a-reinforcing-filler-in-polyurethanes

Liu, D., Zhong, T., Chang, P. R., Li, K. & Wu, Q. (2010). Starch composites reinforced by bamboo cellulosic crystals. *Bioresource Technology*, *101*, 2529–2536.

Liu, H. H., Zhang, L., Li, J. D., Zou, Q., Zuo, Y., Tian, W. D., et al. (2010). Physicochemical and biological properties of nano-hydroxyapatite-reinforced aliphatic polyurethanes membranes. *Journal of Biomaterials Science Polymer Edition*, *21*, 1619–1636.

Ljungberg, N., Cavaillé, J. Y. & Heux, L. (2006). Nanocomposites of isotactic polypropylene reinforced with rod-like cellulose whiskers. *Polymer*, *47*, 6285–6292.

Luo, Wang & Ying. (1997). Hydrogen-bonding properties of segmented polyether poly(urethane urea) copolymer. *Macromolecules*, *30*, 4405–4409.

Maafi, E. M., Tighzert, L. & Malek, F. (2010). Elaboration and characterization of composites of castor oil-based polyurethane and fibers from alfa stems. *Journal of Applied Polymer Science*, *118*, 902–909.

Mathew, A. P., Thielemans, W. & Dufresne, A. (2008). Mechanical properties of nanocomposites from sorbitol plasticized starch and tunicin whiskers. *Journal of Applied Polymer Science*, *109*, 4065–4074.

Mattia, J. & Painter, P. (2007). A comparison of hydrogen bonding and order in a polyurethane and poly(urethane-urea) and their blends with poly(ethylene glycol). *Macromolecules*, *40*, 1546–1554.

Noble, K. L. (1997). Waterborne polyurethanes. *Progress in Organic Coatings*, *32*, 131–136.

Oprea, S. (2010). Dependence of fungal biodegradation of PEG/castor oil-based polyurethane elastomers on the hard-segment structure. *Polymer Degradation and Stability*, *95*, 2396–2404.

Ozgurseydibeyoglu, M. & Oksman, K. (2008). Novel nanocomposites based on polyurethane and micro fibrillated cellulose. *Composites Science and Technology*, *68*, 908–914.

Pei, A., Malho, J.-M., Ruokolainen, J., Zhou, Q. & Berglund, L. A. (2011). Strong nanocomposite reinforcement effects in polyurethane elastomer with low volume fraction of cellulose nanocrystals. *Macromolecules*, *44*, 4422–4427.

Senich, G. A. & MacKnight, W. J. (1980). Fourier transform infrared thermal analysis of a segmented polyurethane. *Macromolecules*, *13*, 106–110.

Seo, J. W. & Kim, B. K. (2005). Preparations and properties of waterborne polyurethane/nanosilica composites. *Polymer Bulletin*, *54*, 123–128.

Siro, I. & Plackett, D. (2010). Microfibrillated cellulose and new nanocomposite materials: A review. *Cellulose*, *17*, 459–494.

Syverud, K., Chinga-Carrasco, G., Toledo, J. & Toledo, P. G. (2011). A comparative study of Eucalyptus and *Pinus radiata* pulp fibres as raw materials for production of cellulose nanofibrils. *Carbohydrate Polymers*, *84*, 1033–1038.

Tan, S. G. & Chow, W. S. (2010). Biobased epoxidized vegetable oils and its greener epoxy blends: A review. *Polymer Plastics Technology and Engineering*, *49*, 1581–1590.

Teixeira, E. D., Lotti, C., Correa, A. C., Teodoro, K. B. R., Marconcini, J. M. & Mattoso, L. H. C. (2011). Thermoplastic corn starch reinforced with cotton cellulose nanofibers. *Journal of Applied Polymer Science*, *120*, 2428–2433.

Wang, Y. X., Cao, X. D. & Zhang, L. N. (2006). Effects of cellulose whiskers on properties of soy protein thermoplastics. *Macromolecular Bioscience*, *6*, 524–531.

Wu, Q., Henriksson, M., Liu, X. & Berglund, L. A. (2007). A high strength nanocomposite based on microcrystalline cellulose and polyurethane. *Biomacromolecules*, *8*, 3687–3692.

Yeganeh, H. & Hojatitalemi, P. (2007). Preparation and properties of novel biodegradable polyurethane networks based on castor oil and poly(ethylene glycol). *Polymer Degradation and Stability*, *92*, 480–489.

Yoon, S. C., Sung, Y. K. & Ratner, B. D. (1990). Surface and bulk structure of segmented poly(ether urethanes) with perfluoro chain extenders. 4. Role of hydrogen bonding on thermal transitions. *Macromolecules*, *23*, 4351–4356.

Yoon, S.-S., Kim, J.-H. & Kim, S.-C. (2005). Synthesis of biodegradable PU/PEGDA IPNs having micro-separated morphology for enhanced blood compatibility. *Polymer Bulletin*, *53*, 339–347.

Zhang, Y., Wang, J., Zhao, Y., Kang, M. & Wang, X. (2006). Mechanical properties and morphology of the clay/waterborne polyurethane nanocomposite. *Journal of Wuhan University of Technology Materials Science Edition*, *21*, 24–27.

Zhang, Y., You, B., Huang, H., Zhou, S., Wu, L. & Sharma, A. (2008). Preparation of nanosilica reinforced waterborne silylated polyether adhesive with high shear strength. *Journal of Applied Polymer Science*, *109*, 2434–2441.

Zou, J., Zhang, F., Huang, J., Chang, P. R., Su, Z. & Yu, J. (2011). Effects of starch nanocrystals on structure and properties of waterborne polyurethane-based composites. *Carbohydrate Polymers*, *85*, 824–831.